Materials Research Proceedings **2** (2016) 73-78 doi: http://dx.doi.org/10.21741/9781945291173-13

3D Residual Stresses in Selective Laser Melted Hastelloy X

Jonas Saarimäki[†, 1, a, *], Mattias Lundberg[†, 1, b], Johan J. Moverare[1, c], Håkan Brodin[2, d]

[1]Department of Management and Engineering, Division of Engineering materials, Linköping University, Linköping, SE-58183, Sweden

[2]Siemens Industrial Turbomachinery AB, Finspång, SE-612 31, Sweden

[†]Joint first author

[a]Jonas.saarimaki@liu.se, [b]mattias.lundberg@liu.se, [c]johan.moverare@liu.se, [d]hakan.brodin@siemens.com

Keyword: Triaxial Stress, SLM, HX

Abstract. 3D residual stresses in as manufactured EOS NickelAlloy HX, produced by laser powder bed additive manufacturing, are analysed on the surface closest to the build-plate. Due to the severe thermal gradient produced during the melting and solidification process, profound amounts of thermal strains are generated. Which can result in unwanted geometrical distortion and effect the mechanical properties of the manufactured component. Measurements were performed using a four-circle goniometer Seifert X-ray machine, equipped with a linear sensitive detector and a Cr-tube. Evaluation of the residual stresses was conducted using $sin^2\psi$ method of the Ni {220} diffraction peak, together with material removal technique to obtain in-depth profiles. An analysis of the material is reported. The analysis reveals unwanted residual stresses, and a complicated non-uniform grain structure containing large grains with multiple low angle grain boundaries together with nano-sized grains. Grains are to a large extent, not equiaxed, but rather elongated.

Introduction

Additive manufacturing, free form fabrication, rapid prototyping and 3D-printing are some of the different designations for processes where components can be built to finished or near-finished shape without machining a block of material or casting material in a mould [1–3]. The processes were primarily developed for simpler materials, such as thermoset plastics and plaster. The lasers equipment originally used could only melt materials with low melting points, for instance brass, and was not powerful enough to completely melt steel. Therefore, this manufacturing method could not meet the requirements for parts subjected to high stress levels or elevated temperatures, e.g., superalloys [4]. With time, the process control was improved and more powerful lasers were developed. With the higher input possible from a more powerful laser it is possible to create a microstructure with a low amount of porosity and no internal defects such as solidification cracks or poor bonding [5].

Free-form fabrication of superalloys is gaining increased interest from the industry, since the available range of alloys is growing. Today, alloys for selective laser melting (SLM) include aluminium, titanium, tool steel, stainless steel and heat resistant materials of cobalt- and nickel-base. In the case of melting of metal powders, the dominating manufacturing process is laser melting, often denoted selective laser melting, direct laser metal sintering (DMLS) or LaserCUSING. All of these names are trademarks for different companies manufacturing equipment for laser melting.

The laser melting manufacturing process can briefly be described as a layer-by layer process, where powder is distributed on a powder bed, see Fig. 1. Firstly, a powder distributer travels over the powder bed cavity contained by the build chamber walls and build plate. Molten and solidified

Materials Research Proceedings **2** (2016) 73-78 doi: http://dx.doi.org/10.21741/9781945291173-13

powder constitutes the component surrounded by un-molten powder. Secondly, a laser beam melts the powder layer and creates a new slice of solid material in the component. Thirdly, a ram lowers the build platform and the process is repeated until a finished geometry is formed. After finalisation, the remaining loose powder is removed and the component is cut off from the build platform.

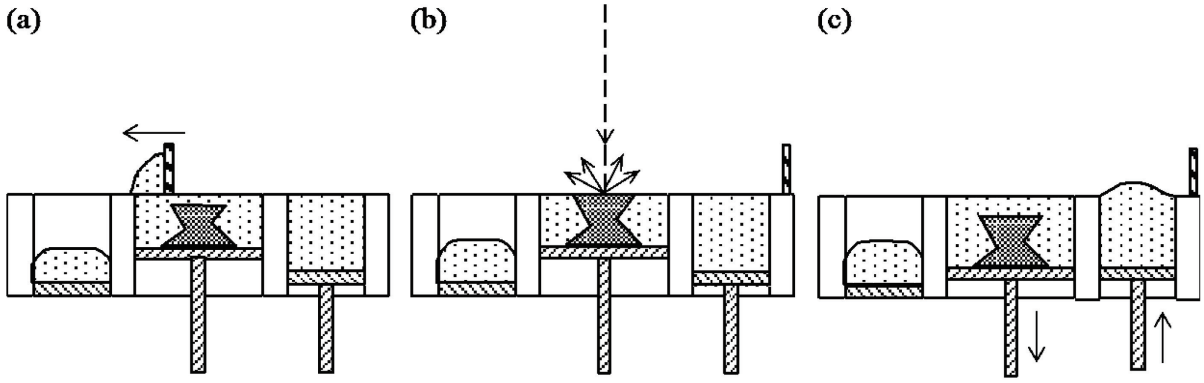

Figure 1. Schematic description of the SLM process. (a) Powder is distributed on a powder bed, the build platform. (b) The powder is melted by a laser beam and a slice of solid metal is formed. (c) The powder bed is lowered and the process is repeated until a finished component is formed.

Although selective laser melting allows manufacturing of complex geometries, it comes with drawbacks compared to the conventional manufacturing technologies. The temperature gradient and consequent plastic deformation leads to residual stresses and deformation due to the locally focused energy input [6]. Residual stresses can influence the geometrical accuracy and mechanical strength as well as contribute to crack initiation. Previous research has been conducted using methods such as the crack compliance method which is not suited for near surface stresses [7], hole drilling which requires large dimensional sizes and smooth surfaces to be effective [8]. In this study, x-ray diffraction was used to measure surface and bulk stresses using material removal technique.

The purpose of this study is to examine residual stress levels in as manufactured SLM material. No post processing or heat treatments were done prior to testing since gas atomised EOS NickelAlloy HX powder is used for manufacturing e.g., gas turbine burners used in the as manufactured state.

Experimental details

The material used in the current study is manufactured from powder EOS NickelAlloy HX. In literature Hastelloy X can be identified as Alloy X, when not available from the original manufacturer. The powder material is gas atomized and sieved to a fraction (10−45 μm) suitable for the SLM process. After manufacturing no post-processing, such as heat treatment or hot isostatic pressing, was conducted. The nominal composition in wt.% of EOS NickelAlloy HX is shown in Table 1. During the SLM manufacturing the test specimen was attached to the building platform via area A in Fig. 2. After manufacturing, the test specimen was removed from the platform by wire electro discharge machining. The typical microstructure of the laser melted material after manufacturing is shown in Fig. 3-4, where the building direction is indicated by the arrows. Previous work by Brodin *et al*. [9] on alloy X has shown that material bulk properties meet or exceed the properties of both hot-rolled and cast Hastelloy X in heat treated condition.

Table 1. Chemical composition, EOS NickelAlloy HX [wt.%].

Ni	Cr	Fe	Mo	W	Co	C	Si
Bal.	20.5−23.0	17.0−20.0	8.0−10.0	0.2−1.0	0.5−2.5	≤0.1	≤0.1
Mn	S	P	B	Se	Cu	Al	Ti
≤0.1	≤0.03	≤0.04	≤0.01	≤0.005	≤0.5	≤0.5	≤0.15

Materials Research Proceedings **2** (2016) 73-78 doi: http://dx.doi.org/10.21741/9781945291173-13

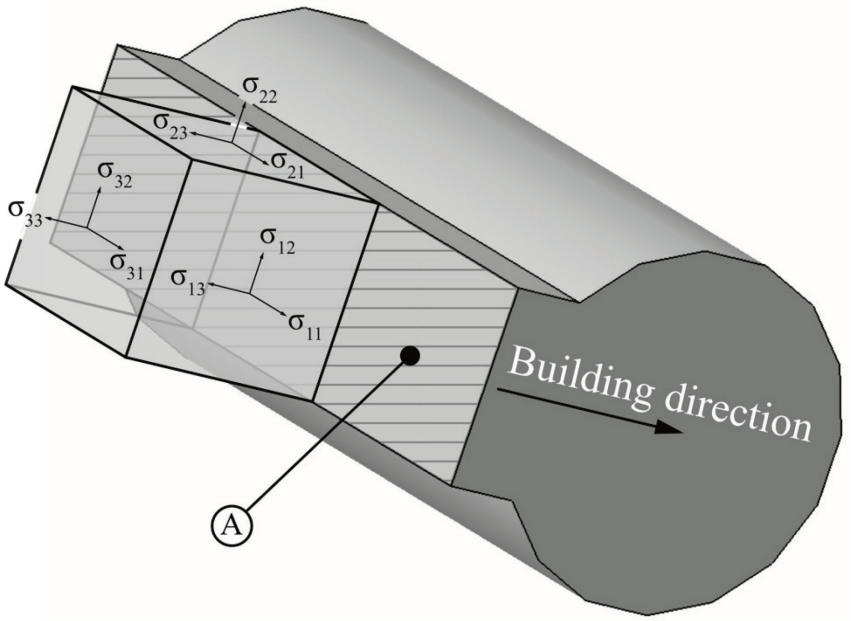

Figure 2. Sample geometry and stress components where A denotes build plate attachment area and the arrow the building direction.

Triaxial X-ray measurements [10] were performed using a four-circle goniometer Seifert X-ray machine, equipped with a linear sensitive detector, Cr-tube and a 2 mm spot collimator. The {220} diffraction peak of γ-phase was used for the stress measurement with the *sin²ψ*-method. Values off the x-ray elastic constants used were calculated using the Young's modulus (190 GPa) and Poison's ratio (0.31) based on the work by Saarimäki [11] resulting in: $s_1 = -1.63\times10^{-6}$ and $½s_2 = 6.89 \times 10^{-6}$ MPa. Which differ from the experimental work on single crystal Hastelloy X [12]. Raw powder from the distributor was used and analysed for two ϕ angles (D1 = 0° and D2 = 90°) together with 13 ψ angles, evenly distributed between ± 60° to determine the unstressed lattice spacing, d_0. No corrections were made considering the stress redistribution due to material removal. The orientation imaging map (OIM) in Fig. 4 was obtained using electron backscatter diffraction (EBSD) with a step size of 1.5 μm and 15 kV in a Hitachi SU70 FEG analytical scanning electron microscope (SEM).

Results

The EBSD analysis revealed a complicated non-uniform grain structure containing large grains with several low angle grain boundaries together with nano-sized grains. Grains are to a large extent, not equiaxed, but rather elongated, depicted in Fig. 3-4.

Stress free lattice spacing, d_0, determination [13] of the gas atomized powder is shown in Fig. 5. The stress free lattice spacing d_0 was calculated by fitting two linear models and computing the intersect point, resulting in $d_0 = 1.2728$ Å.

The directional grains could cause a crystallographic texture as well as anisotropy leading to the non-linear behaviour seen in Fig. 6.

Initial surface measurements in Fig. 7 reveal large tensile stresses (σ_{11} = 660 MPa, σ_{22} = 740 MPa, σ_{33} = 755 MPa). A steep gradient is evident from the surface to a depth of ~20 μm, with the lowest residual stresses obtained in the principal directions (σ_{11}= -70 MPa, σ_{22} = 30 MPa,

σ_{33} = 100 MPa). From 20 − 45 μm, the stress in the σ_{11} direction increase greatly. After this depth the changes in stresses reduces and are fairly stable in value. At 445 μm depth, the residual stresses in the principal directions are as follows: σ_{11}= 400 MPa, σ_{22} = 90 MPa and σ_{33} = 85 MPa.

σ_{12} shows compressive stresses at the surface which approaches zero stress level at 445 μm. Little or no shear stresses were calculated for σ_{13} and σ_{23}.

Materials Research Proceedings **2** (2016) 73-78 doi: http://dx.doi.org/10.21741/9781945291173-13

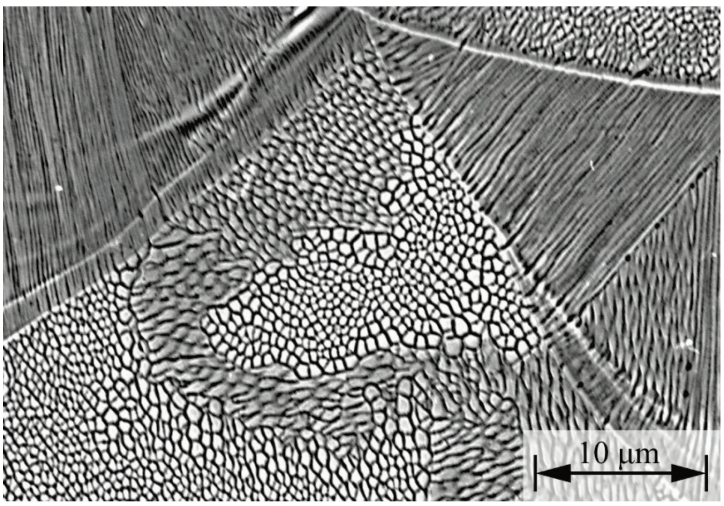

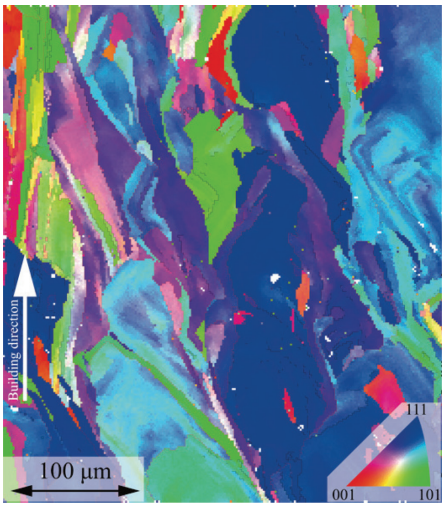

Figure 3. Bulk microstructure comprising cellular dendrites. Figure 4. Orientation imaging map.

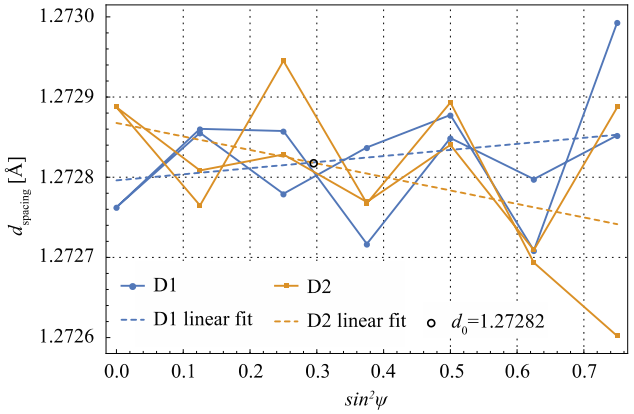

Figure 5. d_0 determination.

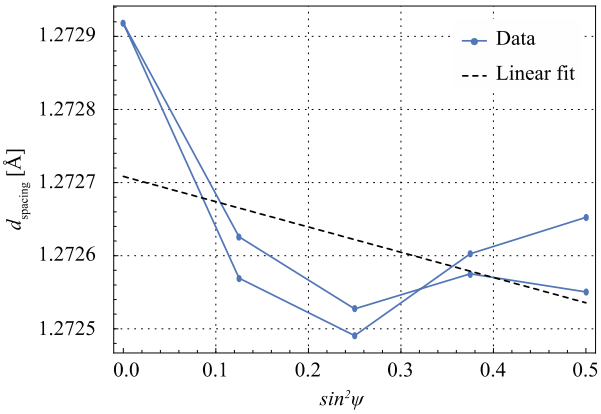

Figure 6. $d_{spacing}$ vs. $sin^2\psi$ at 45 µm and ϕ = 45°.

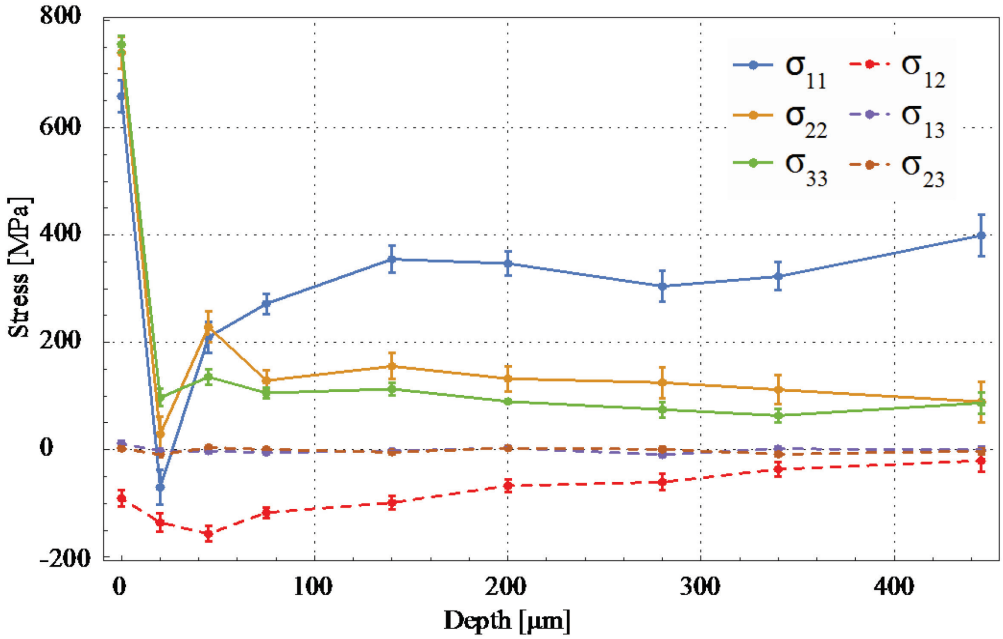

Figure 7. Residual stress profile.

Materials Research Proceedings **2** (2016) 73-78 doi: http://dx.doi.org/10.21741/9781945291173-13

Discussion

Electron backscatter diffraction together with an OIM was used to analyse the microstructure in Fig. 3-4. The analysis revealed a non-uniform grain structure containing large elongated (not equiaxed) grains with many low angle grain boundaries together with nano-sized grains. The grains are oriented directionally, parallel to the building direction giving this unconventional microstructure. The directional grains could cause a crystallographic texture as well as anisotropy leading to the non-linear behaviour in Fig. 6.

The gas atomised powder used to determine the stress free lattice spacing d_0 was not completely stress free, as seen in Fig. 5. The D1 linear fit has a positive slope and the D2 linear fit has a negative slope. The presence of residual stresses is likely due to the rapid cooling from molten to solid state since the powder is gas atomised. The assumption to use the gas atomised powder for d_0 determination is reasonable since both the powder and the alloy are free from precipitates. Furthermore, the cellular dendritic SLM material and the dendrites in the gas atomised powder particles have similar primary dendrite arm spacing's.

The residual stresses in the specimen are significant since warping of the specimen is seen just by looking at it. The high surface residual stress values (σ_{11}= 660 MPa, σ_{22}= 740 MPa, σ_{33}= 755 MPa) shown in Fig. 7 are above the yield stress but lower than the tensile strength (676 MPa in the relevant direction, i.e., horizontal), as reported by Brodin and Saarimäki [14]. Electric discharge machining, can change the microstructure to a depth of 5 − 10 μm. This could generate the steep stress gradient observed at the first measured points. Within the measured volume, all stresses except σ_{11} decrease from 145 μm to a depth of 440 μm at which the stresses are fairly stable. Even though the residual stresses should approach zero and eventually become compressive in the bulk, the stresses extend to a greater depth than investigated here. The high σ_{11}stress level is responsible for the specimen deformation caused by the layer by layer build process during solidification and cooling.

Biaxial stress state assumes that there is a linear relationship between d_{spacing} and $sin^2\psi$ [15]. However, a biaxial stress state cannot be assumed in this case since in depth and shear components are ≠ 0 which results in the poor linear fit in Fig. 6. Thus, the triaxial stress calculations performed are believed to better reflect the actual stress state in the specimen.

Due to the lack of data regarding the x-ray elastic constants (XEC) s_1 and $½s_2$, they were calculated using the Young's modulus (bulk parameter) and ν. However, these calculated values could render non-negligible errors. Using the XEC for single crystal Hastelloy X [12] or Inconel 718 [16] would generate a shift in measured stresses of approximately 30 %. Hence, accurate XEC need to be determined.

Conclusions

Residual stress measurements and microstructural analysis was conducted on SLM material from EOS NickelAlloy HX powder. We show that the microstructure is fine-grained and the grains are elongated along the build direction. It is clear that the grains are allowed to grow over several layers during the building process. Electric discharge machining locally changes the microstructure resulting in the steep decline in residual stress from the surface (0 − 20 μm).

All stresses except σ_{11} decrease from 145 μm to a depth of 440 μm where σ_{11} is still increasing. Assuming a biaxial stress state is misleading since the SLM process induce large out of plane residual stresses. Accurate XEC need to be determined due to the lack of data regarding the x-ray elastic constants (XEC) s_1 and $½s_2$ for SLM EOS NickelAlloy HX.

Acknowledgements

The authors would like to thank Agora Materiae, graduate school, Faculty grant SFO-MAT-LiU#2009-00971, and the project teams at Linköping University, Siemens Industrial Turbomachinery AB for valuable discussions.

References

[1] J. Chu, S. Engelbrecht, G. Graf, D.W. Rosen, A Comparison of Synthesis Methods for Cellular Structures with Application to Additive Manufacturing, Rapid Prototyp. J. 16 (2010) 275–283. *http://dx.doi.org/10.1108/13552541080000501*

[2] D.W. Rosen, Computer-Aided Design for Additive Manufacturing of Cellular Structures, Comput. Aided. Des. Appl. 4 (2007) 585–594. doi:10.1080/16864360.2007.10738493. *http://dx.doi.org/10.1080/16864360.2007.10738493*

[3] G. Marchelli, R. Prabhakar, D. Storti, M. Ganter, The guide to glass 3D printing: developments, methods, diagnostics and results, Rapid Prototyp. J. 17 (2011) 187–194. *http://dx.doi.org/10.1108/13552541111124761*

[4] S. Das, J.J. Beaman, M. Wohlert, D.L. Bourell, Direct laser freeform fabrication of high performance metal components The authors, Rapid Prototyp. J. 4 (1998) 112–117. *http://dx.doi.org/10.1108/13552549810222939*

[5] M. Agarwala, D. Bourell, J. Beaman, H. Marcus, J. Barlow, Direct selective laser sintering of metals, Rapid Prototyp. J. 1 (1995) 26–36. doi:10.1108/13552549510078113. *http://dx.doi.org/10.1108/13552549510078113*

[6] P.J. Withers, H.K.D.H. Bhadeshia, Residual stress. Part 2 – Nature and origins, Mater. Sci. Technol. 17 (2001) 366–375. doi:10.1179/026708301101510087. *http://dx.doi.org/10.1179/026708301101510087*

[7] P. Mercelis, J.-P. Kruth, Residual stresses in selective laser sintering and selective laser melting, Rapid Prototyp. J. 12 (2006) 254–265. doi:10.1108/13552540610707013. *http://dx.doi.org/10.1108/13552540610707013*

[8] C. Casavola, S.L. Campanelli, C. Pappalettere, Preliminary investigation on distribution of residual stress generated by the selective laser melting process, J. Strain Anal. Eng. Des. 44 (2009) 93–104. doi:10.1243/03093247JSA464. *http://dx.doi.org/10.1243/03093247JSA464*

[9] H. Brodin, O. Andersson, S. Johansson, Mechanical Behaviour and Microstructure Correlation in a Selective Laser Melted Superalloy, in: ASME Turbo Expo 2013 Turbine Tech. Conf. Expo., San Antonio, Texas, USA, 2013. doi:10.1115/GT2013-95878. *http://dx.doi.org/10.1115/GT2013-95878*

[10] H. Dölle, The influence of multiaxial stress states, stress gradients and elastic anisotropy on the evaluation of (Residual) stresses by X-rays, J. Appl. Crystallogr. 12 (1979) 489–501. *http://dx.doi.org/10.1107/S0021889879013169*

[11] J. Saarimäki, The mechanical properties of lattice truss structures with load- bearing shells made of selectively laser melted Hastelloy X^{TM}, KTH Royal Institute of Technology, 2011. *http://urn.kb.se/resolve?urn=urn:nbn:se:kth:diva-41320.*

[12] H.A. Canistraro, E.H. Jordan, S. Shixiang, L.H. Favrow, F.A. Reed, Elastic Constants of Single Crystal Hastelloy X at Elevated Temperatures, Trans. ASME. 120 (1998) 242–247. doi:10.1115/1.2812350. *http://dx.doi.org/10.1115/1.2812350*

[13] V.M. Hauk, R.W.M. Oudelhoven, G.J.H. Vaessen, The state of residual stress in the near surface region of homogeneous and heterogeneous materials after grinding, Metall. Trans. A. 13 (1982) 1239–1244. doi:10.1007/BF02645507. *http://dx.doi.org/10.1007/BF02645507*

[14] H. Brodin, J. Saarimäki, Mechanical properties of lattice truss structures made of a selective laser melted superalloy, in: 13th Int. Conf. Fract., Beijing, China, 2013: pp. 1–10. *http://urn.kb.se/resolve?urn=urn:nbn:se:liu:diva-95433.*

[15] I.C. Noyan, J.B. Cohen, Residual stress Measurement by diffraction and Interpretation, 1987.

[16] P.S. Prevey, A method of determening the elastic properties of alloys in selected crystallographic directions for x-ray diffraction residual stress measurement, Adv. X-Ray Anal. 20 (1977) 345–354. *http://dx.doi.org/10.1007/978-1-4613-9981-0_30*